Diluted 3d-Random Field Ising Model at zero temperature with metastable dynamics

Xavier Illa* and Eduard Vives†
Departament d'Estructura i Constituents de la Matèria, Universitat de Barcelona
Martí i Franquès 1, Facultat de Física, 08028 Barcelona, Catalonia
(Dated: February 6, 2008)

We study the influence of vacancy concentration on the behaviour of the three dimensional Random Field Ising model with metastable dynamics. We focus our analysis on the number of spanning avalanches which allows for a clean determination of the critical line where the hysteresis loops change from continuous to discontinuous. By a detailed finite size scaling analysis we determine the phase diagram and estimate numerically the critical exponents along the whole critical line. Finally we discuss the origin of the curvature of the critical line at high vacancy concentration.

PACS numbers: 75.40.Mg, 75.50.Lk, 05.50.+q, 75.10.Nr, 75.60.Ej

I. INTRODUCTION

Externally driven systems at low enough temperature often display rate independent hysteresis. This out-of-equilibrium phenomenon occurs because intrinsic disorder creates multiple energy barriers that the system cannot overcome due to the very weak thermal fluctuations.

The study of zero temperature models with metastable dynamics has been very succesful for understanding rate independent hysteresis. A prototype case is the Random Field Ising Model (RFIM) with single spin-flip relaxation dynamics [1, 2]. Although the model is formulated in terms of magnetic variables (external field H and magnetization m) it can be applied to the study of many phenomena associated to low temperature first-order phase transitions in disordered systems, e.g. martensitic transformations [3], fluid adsorption in porous solids [4], ferroelectrics [5], etc.

Disorder is a intriguing concept: in the RFIM it is introduced via independent and quenched random fields on each lattice site, gaussian distributed with zero mean and standard deviation σ. In real materials, disorder is much more complicated and includes features at all length scales: vacancies, interstitials, composition fluctuations, dislocations, strain fields, grain boundaries, sample surfaces, edges and corners, etc. Thus it is interesting to add to the RFIM other sources of disorder in order to see how the non-equilibrium behaviour is modified.

The goal of this paper is to study the diluted RFIM at $T = 0$ with metastable dynamics and analyze the consequence of introducing a concentration c of quenched vacancies. The interplay between the two kinds of disorder (random fields and vacancies) will be at the origin of the properties of the $\sigma - c$ phase diagram.

One of the striking results concerning the RFIM with metastable dynamics, as already pointed out in the seminal paper of Sethna et al.[1], is the occurence of a critical point when the amount of disorder σ is increased. The m vs. H hysteresis loops change from discontinuous (like in a ferromagnet) when $\sigma < \sigma_c$ to continuous (like in a spin-glass) when $\sigma > \sigma_c$. This result was demonstrated using mean-field analysis and numerical simulations in 3d systems. This problem was also studied within the Renormalization Group formalism [6, 7]. Moreover, many properties of the critical point have been also studied analytically on Bethe lattices [8, 9, 10, 11, 12]. Experimental evidence for the occurence of such a critical point has been found in different magnetic systems [13, 14].

Another interesting result of the RFIM with metastable dynamics is that it reproduces the experimental observation that the $m(H)$ trajectories of such athermal systems are discontinuous at small scales. The evolution proceeds by avalanches from a mestastable state to another. In the RFIM the avalanche size distribution becomes a power-law at the critical point. Experimentally, scale free distributions of avalanche properties have been found in many systems [15, 16, 17, 18, 19, 20, 21, 22]. A first attempt to study the influence of dilution in such avalanche size distributions was done some years ago [23]. The results of this work, however, should be considered as only qualitative, given the fact that the studied system was two-dimensional [28], the analysis focused only on the avalanche distributions and the results concerning the phase diagram were very approximate.

The order parameter that vanishes at the critical point is the size of the macroscopic discontinuity Δm. The analysis of this quantity from simulations is very intrincate. In finite-size systems it is very difficult to make the distinction between a macroscopic jump and a microscopic avalanche. The measured order parameter only displays reasonable finite-size scaling (FSS) properties when the simulated systems are very large [24]. Recent studies [25, 26], have shown how the critical point can be characterized in systems of moderate size. The key point is to detect the so-called "spanning" avalanches which are the magnetization jumps that involve a set of spins that spans the whole finite system (e.g. cubic lattice) from one face to the opposite one. By this method avalanches in finite systems can be classified as non-spanning, 1D-spanning, 2D-spanning, or 3D-spanning. The average numbers N_1, N_2 of 1D and 2D-spanning avalanches dis-

*Electronic address: xit@ecm.ub.es
†Electronic address: eduard@ecm.ub.es

play a peak at a value of σ that shifts with system size L and tends to σ_c when $L \to \infty$. The numerical data can then be scaled according to the FSS hypothesis[25]

$$N_\alpha = L^\theta \tilde{N}_\alpha(uL^{1/\nu}) \quad (1)$$

where $\alpha = 1, 2$. The exponent $\nu = 1.2 \pm 0.1$ characterizes the divergence of the correlation length ($\xi \sim (\sigma - \sigma_c)^{-\nu}$) whereas $\theta = 0.10 \pm 0.02$ characterizes the divergence of the number of critical avalanches. The scaling variable $u(\sigma)$ is analytic and measures the distance to the critical point. It can be fitted by the second order expression

$$u(\sigma) = \frac{\sigma - \sigma_c}{\sigma_c} + A\left(\frac{\sigma - \sigma_c}{\sigma_c}\right)^2 \quad (2)$$

with $\sigma_c = 2.21$ and $A = -0.2$. The behaviour of the 3D-spanning avalanches is more complex because they are of two different kinds: (i) critical 3D-spanning avalanches that behave like the 1D and 2D ones and (ii) subcritical 3D-spanning avalanches that will corespond to the Δm discontinuity in the thermodynamic limit. The analysis is more difficult and requires a double finite-size-scaling technique. This will not be used in the present paper. Instead we will focus only on the behaviour of the average numbers N_1 and N_2 in the presence of vacancies and propose a FSS hypothesis by using a bivariate scaling variable $u(\sigma, c)$ that allows to study the full $\sigma - c$ diagram.

In section II, we define the model and the dynamics. In section III, we present results of the numerical simulations. In section IV, we formulate the FSS hypothesis and determine the critical line. In section V, we propose approximations to the bivariate scaling variable $u(\sigma, c)$. In section VI, we discuss the interplay between vacancies and avalanches and finally, in section VII, we summarize our main findings and conclude.

II. MODEL AND SIMULATIONS

The diluted 3D-RFIM on a cubic lattice with N sites ($N = L \times L \times L$) is defined by the following Hamiltonian (magnetic enthalpy):

$$\mathcal{H} = -\sum_{\langle ij \rangle}^{n.n.} c_i c_j S_i S_j - \sum_{i=1}^{N} h_i c_i S_i - H \sum_{i=1}^{N} S_i c_i \quad (3)$$

where $S_i = \pm 1$ are Ising spin variables, $c_i = 0, 1$ indicates the presence of a vacancy ($c_i = 0$) or not ($c_i = 1$) on each site, h_i are quenched random fields gaussian distributed with zero mean and standard deviation σ and H is the driving field. The first sum extends over all distinct nearest-neighbour (n.n.) pairs. Vacancies are quenched and randomly distributed over the lattice. Their concentration is measured by $c = 1 - \sum_i c_i/N$.

The metastable dynamics is implemented as follows: the system is externally driven by the field H which is adiabatically swept from $-\infty$ where the system is fully negatively magnetized ($S_i = -1$) to $+\infty$. ($S_i = +1$). The spins flip according to a local relaxation dynamical rule,

$$S_i = \text{sign}(\sum_j S_j c_j + h_i + H) \quad (4)$$

where the sum extends over all the n.n. of S_i. When a spin flips, it may trigger an avalanche. The unstable spins are flipped synchronously until a new stable situation is reached.

The hysteresis loop is obtained by computing the magnetization

$$m = \sum_{i=1}^{N} S_i c_i / N \quad (5)$$

as a function of the applied field H. Magnetization avalanches are recorded along the whole increasing field branch and their spanning properties are analyzed by using "mask" vectors (as explained in Ref. 25) that allow to classify them as non-spanning, 1D-spanning, 2D-spanning and 3D-spanning. In this work we shall mainly study the number of spanning avalanches of each kind which are recorded in the full upwards branch. These numbers, N_1, N_2 and N_3 which depend on L, σ and c corresponds to averages over more than 10^4 realizations with different random fields and random vacancy positions. The disorder averages are denoted by the symbol $\langle \cdot \rangle$. We study sytems of sizes ranging from $L = 8$ to $L = 64$ in a number of points on the $\sigma - c$ diagram, as indicated schematically in Fig. 1.

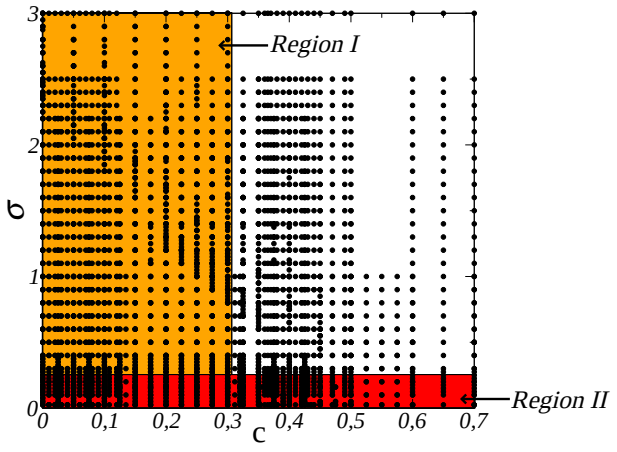

FIG. 1: (Color online) Coordinates of the points studied by numerical simulations in the $\sigma - c$ diagram. The finite size scaling analysis presented in section IV is performed in regions I and II.

III. NUMERICAL RESULTS

The general evolution of the average hysteresis loops as a function of σ and c is shown in Fig. 2. One can observe

the transition from discontinuous loops to smooth loops when σ or c are increased. It can also be seen that the saturation magnetization decreases with increasing c.

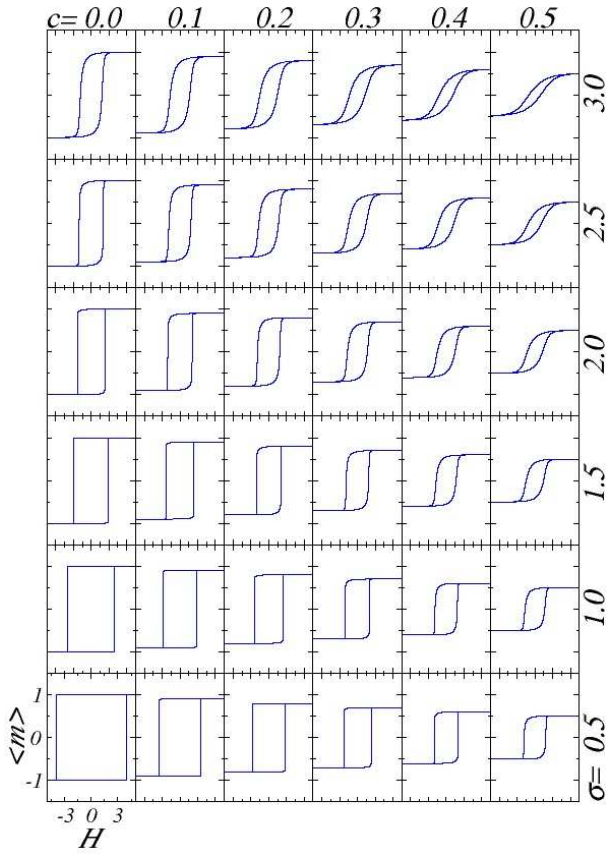

FIG. 2: (Color online) Average hysteresis loops corresponding to a system of size $L = 32$ for different values of σ and c as indicated.

Figure 3 shows the behaviour of the coercive field $\langle H_{coe}\rangle$ as a function of the concentration of vacancies for different values of σ. As can be seen, $\langle H_{coe}\rangle$ decreases with increasing c and increasing σ. The behaviour with increasing c exhibits an inflection point at the transition as can be seen in the inset of Fig. 3 which shows the numerical derivative of the $\langle H_{coe}\rangle$ with respect to c. Such an inflection point does not exist in the non-diluted model when the coercive field is plotted as a function of σ. This feature, which can be of interest for the determination of the critical point in experiments, is probably related to the fact that $\langle H_{coe}\rangle$, as a function of c should vanish at $c \leq 1$ whereas as a function of σ it only vanishes assymptotically when $\sigma \to \infty$.

Fig. 4 shows the distribution $D(s;\sigma,c,L)$ of avalanche sizes (the size s of an avalanche is the number of spins flipped) for the same cases as in Fig. 2 in log-log scale.

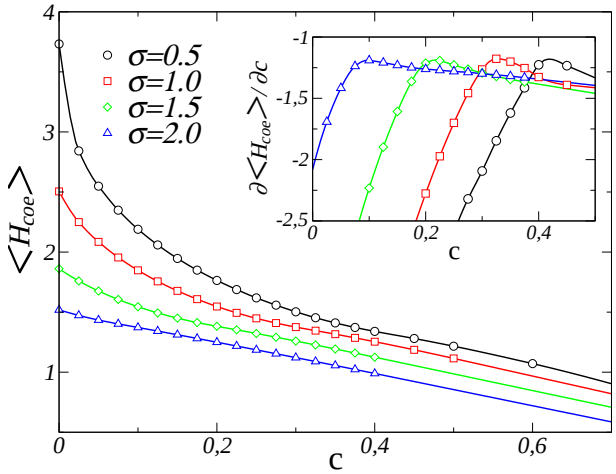

FIG. 3: (Color online) Coercive field as a function of the vacancy concentration c for different values of the amount of disorder σ. The inset shows the behaviour of the numerical derivative $\partial H_{coe}/\partial c$ which exhibits a maximum on the transition line. Data correspond to averages in a system of size $L = 64$.

The histograms include all avalanches irrespective of their spanning properties. The qualitative picture is that power law distributions are obtained along a critical line with an exponent that seems to be the same for all values of c. Apparently, no differences can be observed when comparing the transition induced by changing σ from the transition induced by changing c. Below the critical line the distributions show a peak for large values of s which correspond to the 1D, 2D and 3D spanning avalanches. Above, the distributions have an exponentially damped character.

Figure 5 shows the average number of 1D, 2D and 3D spanning avalanches as a function of σ for increasing values of the vacancy concentration c ranging from 0 to 0.5. Data corresponds to a system with size $L = 16$.

The same information is displayed in Fig. 6 for a system with size $L = 48$.

The behaviour for small and intermediate vacancy concentration is qualitively similar to that found for the non-diluted model [25]. The average numbers N_1 and N_2 display peaks, whereas N_3 shows a peak on the edge of a step function. Note that for $L = 16$ the peak height in $N_1(\sigma,c,L)$ and $N_2(\sigma,c,L)$ seem to decrease with increasing c. This behaviour, however, is much less apparent for larger systems ($L = 48$). Thus, it is possibly due to a finite size effect.

At higher concentrations ($c > 0.4$) N_1 and N_2 begin to develop a flat plateau at low σ. The reason for

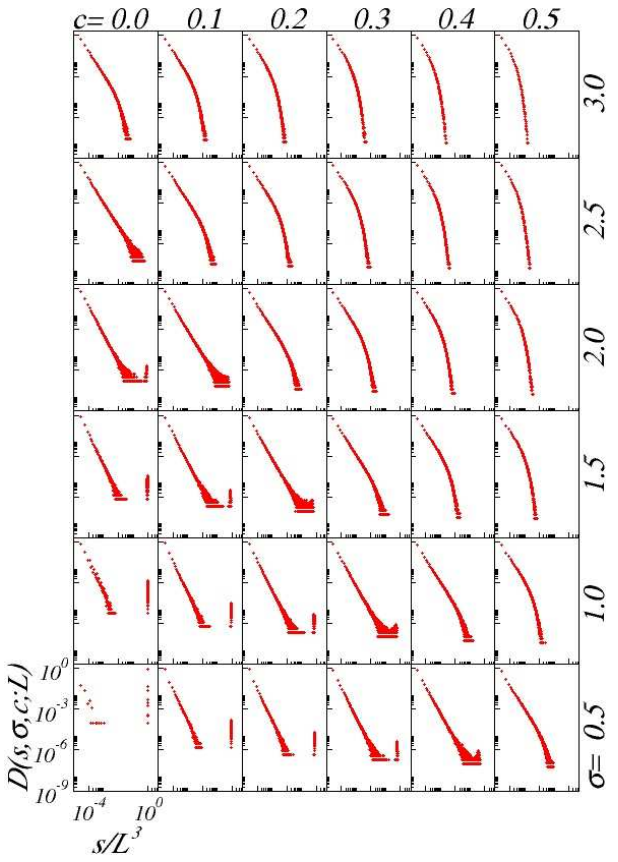

FIG. 4: (Color online) Avalanche size distributions corresponding to a system with $L = 32$ at different values of c and σ as indicated. Data are represented in log-log scale.

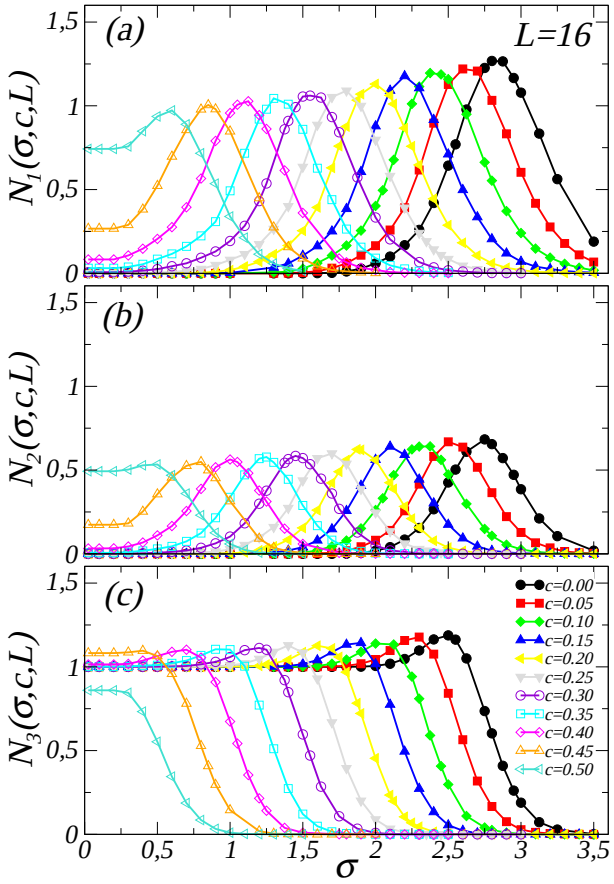

FIG. 5: (Color online) Average number of 1D-spanning avalanches (a), 2D-spanning avalanches (b) and 3D-spanning avalanches (c) as a function of σ for different values of the vacancy concentration c, as indicated by the legend. Lines are guides to the eye. Data corresponds to numerical simulations of a system with size $L = 16$.

this plateau can be well understood by looking at the 3d-plot in Fig. 7, which represents the average number $N_1(\sigma, c, L)$ for $L = 32$. The plateau in the constant c cuts of Figs. 5 and 6 is due to the fact that the crest of the N_1 and N_2 functions bends towards the $\sigma = 0$ axis.

IV. FINITE SIZE SCALING HYPOTHESIS

The hypothesis that we want to check numerically is that, in the presence of vacancies, the critical point found at $c = 0$ transforms into a critical line for a wide range of concentrations. Thus the critical exponents found previously should be equally valid for the description of the behaviour of the average numbers N_1 and N_2 with $c > 0$. According to this hypothesis we shall propose the following corresponding FSS behaviour:

$$N_\alpha(\sigma, c, L) = L^\theta \tilde{N}_\alpha(uL^{1/\nu}) \qquad (6)$$

where $\alpha = 1, 2$ and $u(\sigma, c)$ is a bivariate scaling variable measuring the distance to the critical line. The exponents θ and ν as well as the functions $\tilde{N}_\alpha$ were already found in previous works [25]. Therefore, the hypothesis is quite strong and indicates that all the N_1 and N_2 data corresponding to different sizes L, different vacancy concentrations c and different amounts of disorder σ must collapse into an already known function. The only freedom is in the determination of the bivariate scaling variable u that should be analytic. Before constructing it in the next section, we can make a first test of Eq. 6, by cheking the scaling on the critical line. Note that, setting $u = 0$, Eq. 6 becomes:

$$N_\alpha(\sigma, c, L) = L^\theta \tilde{N}_\alpha(0) \qquad (7)$$

where σ and c should be on the critical line. Since we know (from Ref. 25) that $\theta = 0.10$, $\tilde{N}_1(0) = 0.12$ and $\tilde{N}_2(0) = 0.07$, we can deduce that the different curves $N_\alpha(\sigma, c, L)/L^\theta \tilde{N}_\alpha(0)$ should cross at height 1 on the critical line, independently of L. Two examples are shown in Fig. 8 that corresponds to two cuts (one at constant σ and the other at constant c) in the $\sigma - c$ diagram. As can be seen, the critical line can be determined with high accuracy. By analyzing a large number of such σ and c

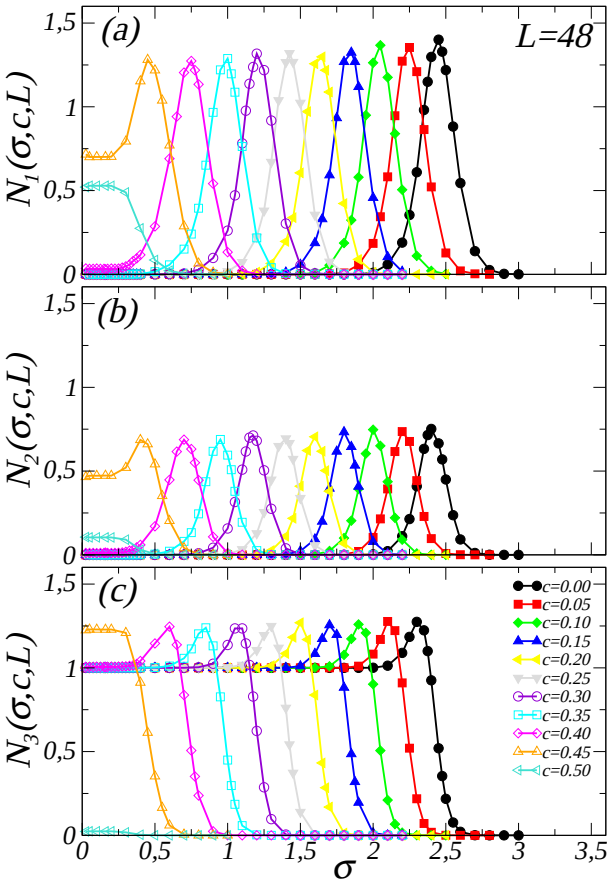

FIG. 6: (Color online) Average number of 1D-spanning avalanches (a), 2D-spanning avalanches (b) and 3D-spanning avalanches (c) as a function of σ for different values of the vacancy concentration c, as indicated by the legend. Lines are guides to the eye. Data corresponds to numerical simulations of a system with size $L = 48$.

cuts we have constructed it. The result is shown in Fig. 9. Note that the process can be repeated independently with N_1 and N_2. The two independent lines overlap almost perfectly.

The obtained critical line is linear up to $c \simeq 0.3$. A least squares fit gives $\sigma_c(c) = \sigma_c(0) + \lambda c$ with $\sigma_c(0) = 2.21 \pm 0.01$ and $\lambda = -4.09 \pm 0.03$. The value $\sigma_c(0) = 2.21$ is in total agreement with the previous estimate for the non-diluted model [25].

It is remarkable that the finite size scaling hypothesis allows the collapse of the data up to large values of c, far from the point $c = 0$ where the scaling function and the exponents where determined. It is also remarkable that scaling works even after the bend that is observed for $c > 0.3$. (Note that the crossing point shown in Fig. 8(a) corresponds to a value of σ where the critical line is not linear.)

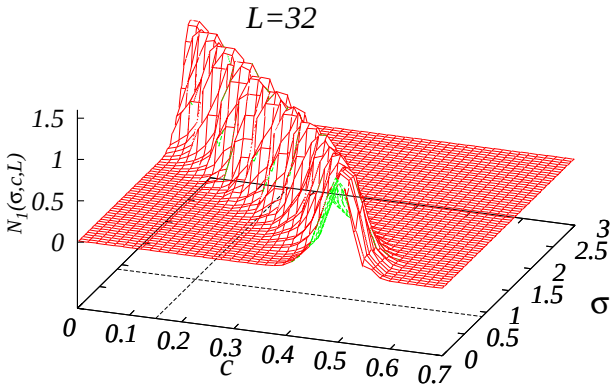

FIG. 7: (Color online) Surface plot representing $N_1(\sigma, c, L)$ for $L = 32$. The dashed lines on the basal plane represent the position of the cuts in Fig.8 at $c = 0.15$ and $\sigma = 0.9$.

For small values of σ, the critical line displays a vertical behaviour. The critical value of the vacancy concentration c_c above which the hysteresis loops do not display a discontinuity can be fitted to $c_c = 0.426 \pm 0.003$

V. BIVARIATE SCALING VARIABLE

In general the bivariate scaling variable is a function that can be expanded as:

$$u(\sigma, c) = a_0 + a_1\sigma + a_2 c + a_3\sigma c + a_4\sigma^2 + a_5 c^2 + \dots \quad (8)$$

Since c and σ are not necessarily very small along the critical line, it is difficult to know a priori how many terms in the expansion will be needed in order to find a good scaling collapse. The direct determination of a large number of coefficients from the numerical data is difficult. Therefore we shall take a different strategy taking into account, as much as possible, the previously known data.

As a first step we will concentrate in the region $c \leq 0.3$ where the coexistence line shows a linear behaviour and we will try to use an expansion up to quadratic terms only. By forcing that the condition $u = 0$ is satisfied on the fitted coexistence line, we deduce that u satisfies:

$$u(\sigma, c) = (\sigma - \sigma_c - \lambda c)(b_0 + b_1\sigma + b_2 c) \quad (9)$$

We should also consider the fact that the scaling variable is known to be well described by a second order expansion (up to σ^2) for $c = 0$ as indicated in Eq. 2. After some algebra one can determine the two parameters b_0 and b_1:

$$b_0 = (1 - A)/\sigma_c = 0.543 \pm 0.002 \quad (10)$$
$$b_1 = A/\sigma_c^2 = -0.041 \pm 0.001 \quad (11)$$

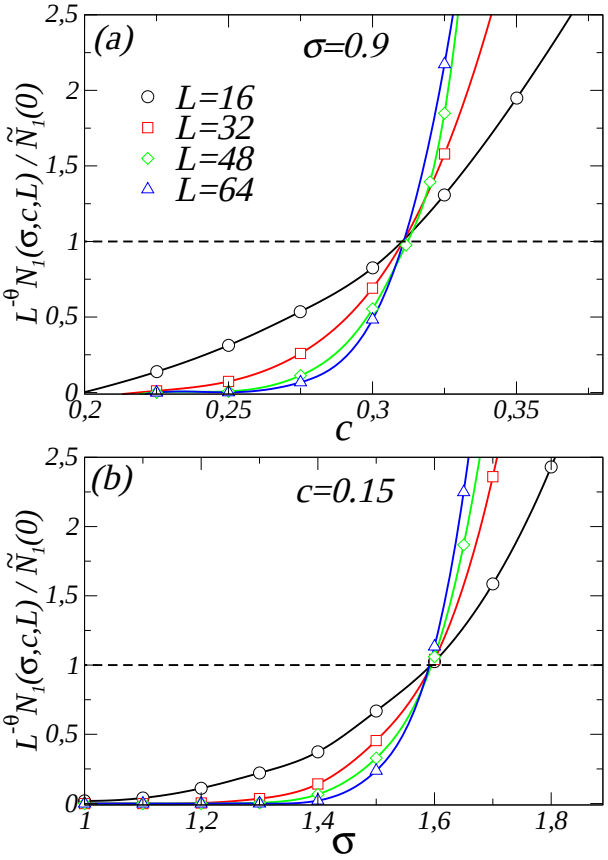

FIG. 8: (Color online) Examples of crossing points on the critical line on cuts (a) parallel to the c axis and (b) parallel to the σ axis. The different symbols correspond to different system sizes as indicated by the legend. Continuous lines are guides to the eye. The horizontal dashed-line indicates the height 1 where the curves are supposed to cross according to Eq. 7.

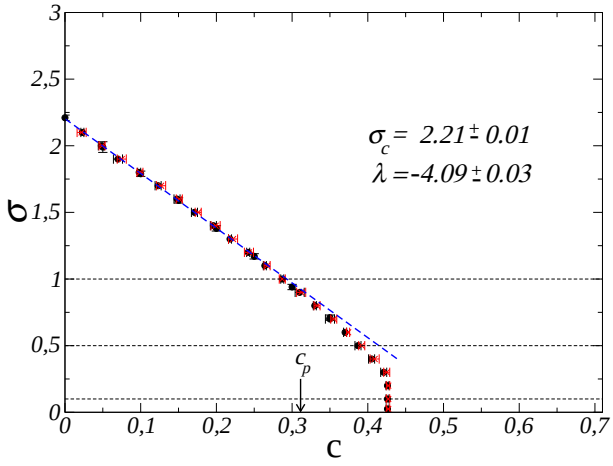

FIG. 9: (Color online) Critical line in the $\sigma - c$ diagram determined from the crossing points in N_1 (•) and N_2 (×). The dashed line is the fit discussed in the text, and the thin discontinuous lines indicate the cuts along which the correlation in Fig. 14 is computed.

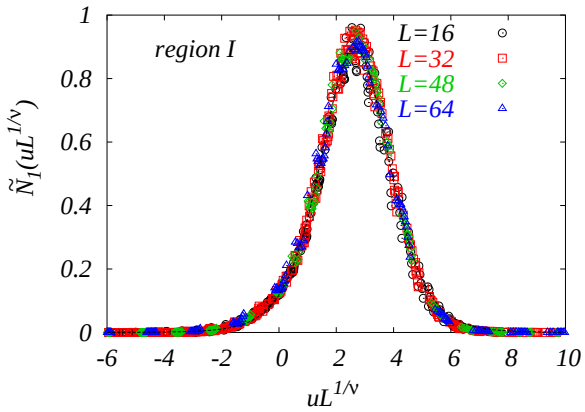

FIG. 10: (Color online) Finite-size-scaling collapse of the average number of 1D-spanning avalanches in region I. The continuous line shows the Lorentzian function in Eq. 12.

Therefore we are left with a single free parameter b_2 that should allow to collapse into a single curve all the data in the scaling region, for different values of σ, c and L. We have considered all the available data in region I of Fig. 1. Note also that the same b_2 parameter must be used to scale both N_1 and N_2 data. The best two collapses are shown in Fig. 10 and Fig. 11 for $b_2 = -0.13$.

Note that the data for $c = 0$ are also included in this plot. Therefore we are obtaining two scaling functions $\tilde{N}_1$ and $\tilde{N}_2$ compatible with those of Ref. 25. In that reference the scaling functions were approximated by Gaussians, although it was also shown that there were systematic deviations. In this work we have tried to fit the data with more complex functions (with three free parameters). We have found a very good χ^2 by using the following modified Lorentzians, which are represented by a continuous line on top of the data in Figs. 10 and 11.

$$\tilde{N}_1(x) = \frac{1}{(1.73 - 0.53x + 0.10x^2)^{3.9}} \qquad (12)$$

$$\tilde{N}_2(x) = \frac{1}{(1.83 - 0.59x + 0.13x^2)^{4.6}} \qquad (13)$$

As a second step we try to build $u(\sigma, c)$ for the data very close to the $\sigma = 0$ axis. In this region II (see Fig. 9) the transition line is again quite linear and in fact is almost vertical. This means that to measure the distance to the critical line it should be sufficient to use the variable $(c - c_c)$. We have considered the following second-order expansion:

$$\frac{u(c)}{k'} = \frac{c - c_c}{c_c} + B\left(\frac{c - c_c}{c_c}\right)^2 \qquad (14)$$

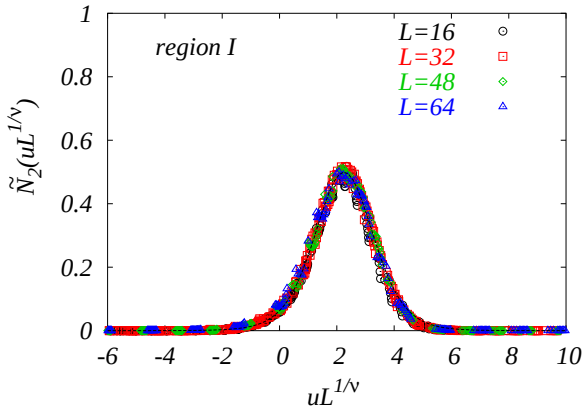

FIG. 11: (Color online) Finite-size-scaling collapse of the average number of 2D-spanning avalanches in region I. The continuous line shows the Lorentzian function in Eq. 13.

Note that k' is not a free parameter. It can be fixed by imposing that the definitions of the scaling variables (9) and (14) coincide at $\sigma = 0$ and $c = 0$. Thus $k' = (A-1)/(B-1)$. The only free parameter for the collapse of the data is B. Best collapses are shown in Fig. 12 and 13 for N_1 and N_2 respectivelly using the best choice $B = -0.2$ (thus $k' = 1$.)

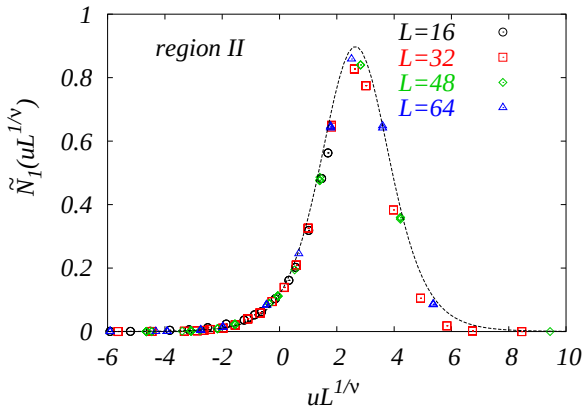

FIG. 12: (Color online) Finite size scaling collapse of the average number of 1D-spanning avalanches in region II. The continuous line shows the lorentzian funcion in Eq. 12.

The continuous lines in both figures correspond to the same lines as in Figs. 10 and 11. We can thus conclude that we have built two good approximations (given by Eq. 9 and 14) in regions I and II, to the unique scaling variable which will display a more complex behaviour in the intermediate region were the critical line bends, probably with higher order terms.

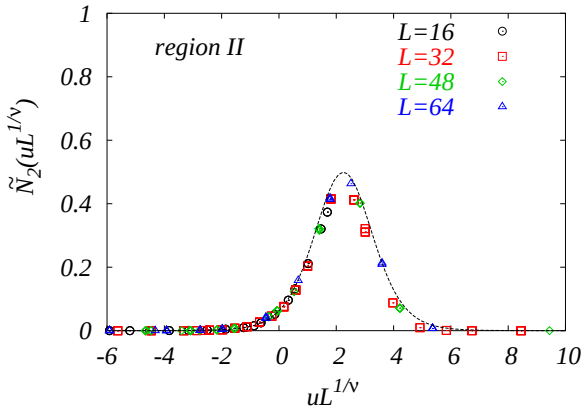

FIG. 13: (Color online) Finite size scaling collapse of the average number of 2D-spanning avalanches in region II. The continuous line shows the lorentzian funcion in Eq. 13.

VI. DISCUSSION

In this section we try to understand why the critical line exhibits such a curvature. There must be a physical reason that goes beyond the mere effect of the dilution of the system and unstabilizes even more the phase with the ferromagnetic-like discontinuity. We propose that the effect is related to the percolation of vacancies above $c_p = 0.3116$, a value which is, indeed, very close to the limit where the critical line loses its linearity. To justify this hypothesis numerically we have studied, for each particular realization of disorder the distribution of the clusters of vacancies and the position of the avalanches. In particular we have determined the spatial position of the largest vacancy cluster (which above c_p will correspond to the percolating cluster in the thermodynamic limit). It is clear that the neigbouring sites of this percolating cluster of vacancies are an easy path for the propagation of an avalanche since these sites have a smaller number of neighbours. To distinghuish such sites we have defined a local flag that takes values $b_i = 1$ when a site belongs to the border of the largest cluster of vacancies or $b_i = 0$ otherwise. We have also recorded the largest avalanche during the H-scan (which will correspond to the spanning avalanche below the critical line in the thermodynamic limit) and marked its position with a flag $\epsilon_i = 1$. With these two variables we have defined the correlation between the border of the largest cluster of vacancies and the largest avalanche as:

$$\rho_{\epsilon,b} = \frac{\langle \frac{1}{N}\sum \epsilon_i b_i\rangle - \langle \frac{1}{N}\sum \epsilon_i\rangle\langle \frac{1}{N}\sum_i b_i\rangle}{\sqrt{\langle \frac{1}{N}\sum \epsilon_i^2\rangle - \langle \frac{1}{N}\sum \epsilon_i\rangle^2}\sqrt{\langle \frac{1}{N}\sum b_i^2\rangle - \langle \frac{1}{N}\sum b_i\rangle^2}} \quad (15)$$

Note that since ϵ_i and b_i take values $1, 0$ only, the power 2 in the first bracket inside the square roots can be suppressed. This correlation is equal to 1 when the spanning

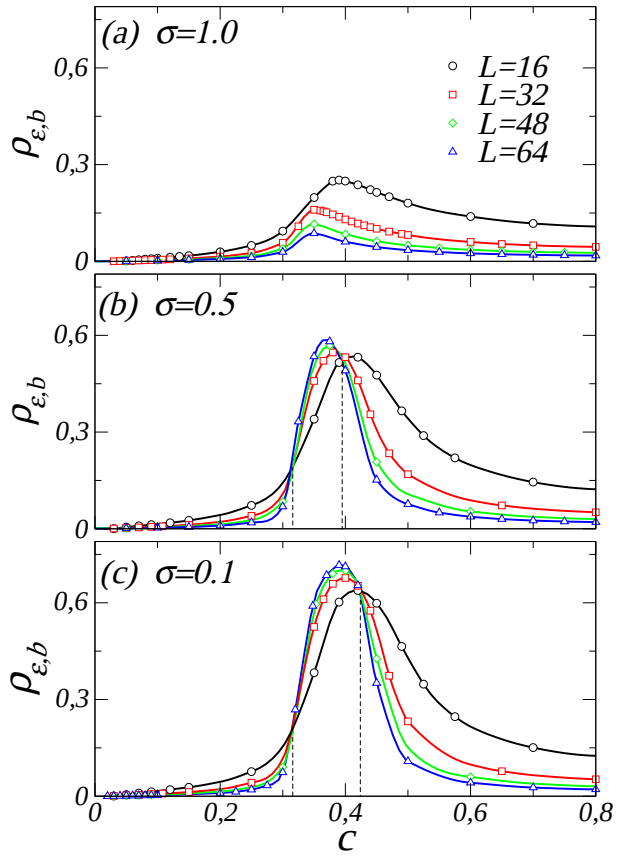

FIG. 14: (Color online) Correlation between the border of the largest cluster of vacancies and the largest avalanche as a function of c. Data corresponding to different system sizes are represented by different symbols as indicated by the legend. The curves correspond to cuts in the phase diagram at $\sigma = 1$ (a), $\sigma = 0.5$ (b) and $\sigma = 0.1$ (c).

avalanche sits exactly on the border of the spanning cluster of vacancies. The behaviour of $\rho_{\epsilon,b}$ as a function of c is shown in Fig. 14 for three different values of σ that correspond to the dashed lines indicated in Fig. 9 and for increasing system sizes as indicated by the legend. The important observation is that the curves for $\sigma = 0.5$ and $\sigma = 0.1$ exhibit two crossing points. One is located at c_p and the other on the critical line (it thus shifts with σ). For a concentration of vacancies below c_p or above the critical line, the behaviour of the curves with increasing L indicates that the correlation vanishes in the thermodynamic limit, whereas in the region between the two crossing points the correlation increases with increasing system size. A value $\rho = 1$ is probably not reached since the spanning avalanche is larger than the border of the percolating cluster of vacancies. By this analysis, we have thus identified the origin of the curvature of the critical line: when vacancies percolate the spanning avalanche propagates along the border of the percolating cluster of vacancies. The propagation in such a constrained environment decreases the amount of disorder needed to break the infinite macroscopic avalanche into small microscopic jumps. However, as shown in the previous section this mechanism does not changes the values of the critical exponents.

VII. SUMMARY AND CONCLUSIONS

We have analyzed the influence of dilution on the critical properties of the 3D-RFIM at $T = 0$ with metastable dynamics. We have shown that the critical point associated to the change in the shape of the hysteresis loop from discontinuous to continuous loops becomes a critical line which we have located in the $\sigma - c$ phase diagram. The critical properties close to this line are characterized by the same critical exponents as in the non-diluted model. This result indicates that it should be possible to find RG arguments showing that there is a unique fixed point at $T = 0$ in the disorder parameter space, that includes, at least, both random fields and dilution [2]. We have computed quadratic approximations to the scaling variable in two different zones of the phase diagram that allow for a bivariate finite-size-scaling collapse on a universal scaling function. Finally we have proposed an explanation for the the curvature observed in the critical line when the concentration of vacancies increases above the percolation limit: the spanning avalanche that is responsible for the discontinuity of the hysteresis loops, has a tendency to follow the neigbourhood of the percolating cluster of vacancies.

VIII. ACKNOWLEDGEMENTS

We acknowledge fruitful discussions with M.L.Rosinberg, F.J.Pérez-Reche and A.Planes. This work has received financial support from projects MAT2004-01291 (CICyT, Spain) and SGR-2001-00066 (Generalitat de Catalunya). X.I. acknowledges a grant from DGI-MEC (Spain).

[1] J. P. Sethna, K. Dahmen, S. Kartha, J. A. Krumhansl, B. W. Roberts, and J. D. Shore, Phys. Rev. Lett. **70**, 3347 (1993).
[2] J.P.Sethna, K.Dahmen, and O.Perković, *The Science of Hysteresis* (Elsevier Inc., 2005), vol. 2, chap. 2, pp. 107–179.
[3] J.Ortín, A.Planes, and L.Delaey, *The Science of Hysteresis* (Elsevier Inc., 2005), vol. 3, chap. 5, pp. 467–541.
[4] F.Detcheverry, E.Kierlik, M.L.Rosinberg, and G.Tarjus, Phys. Rev. E **68**, 061504 (2003).
[5] B.Tadić, Eur. Phys. J. B **28**, 81 (2002).
[6] K. A. Dahmen and J.P.Sethna, Phys. Rev. Lett. **71**, 3222

(1993).
[7] K. A. Dahmen and J.P.Sethna, Phys. Rev. B **53**, 14872 (1996).
[8] D. Dhar, P. Shukla, and J. Sethna, J. Phys. A: Math. Gen. **30**, 5259 (1997).
[9] X.Illa, J.Ortín, and E.Vives, Phys. Rev. B **71**, 184435 (2005).
[10] X.Illa, P.Shukla, and E.Vives, Phys. Rev. B **73**, 092414 (2006).
[11] P. S. S. Sabhapandit and D. Dhar, J. Stat. Phys. **98**, 103 (2000).
[12] P. Shukla, Phys. Rev. E **63**, 027102 (2001).
[13] A.Berger, A.Inomata, J.S.Jiang, J.E.Pearson, and S.D.Bader, Phys. Rev. Lett. **85**, 4176 (2000).
[14] J. Marcos, E. Vives, L. Mañosa, M. Acet, E. Duman, M.Morin, V. Novák, and A. Planes, Phys. Rev. B **67**, 224406 (2003).
[15] K.L.Babcock and R.M.Westervelt, Phys. Rev. Lett. **64**, 2168 (1990).
[16] P.J.Cote and L.V.Meisel, Phys. Rev. Lett. **67**, 1334 (1991).
[17] E. Vives and A. Planes, Phys. Rev. B **50**, 3839 (1994).
[18] W.Wu and P.W.Adams, Phys. Rev. Lett **74**, 610 (1995).
[19] Ll.Carrillo, Ll.Mañosa, J.Ortín, A.Planes, and E.Vives, Phys. Rev. Lett. **81**, 1889 (1998).
[20] E. Puppin, Phys. Rev. Lett. **84**, 5415 (2000).
[21] G.Durin and S.Zapperi, Phys. Rev. Lett. **84**, 4705 (2000).
[22] M.P.Lilly, P.T.Finley, and R.B.Hallock, Phys. Rev. Lett. **71**, 4186 (1993).
[23] B.Tadić, Phys. Rev. Lett. **77**, 3843 (1996).
[24] M. C. Kuntz, O. Perković, K. A. Dahmen, B. Roberts, and J.P.Sethna, Computing in Science & Engineering **July/August**, 73 (1999).
[25] F.J.Pérez-Reche and E.Vives, Phys. Rev. B **67**, 134421 (2003).
[26] F.J.Pérez-Reche and E.Vives, Phys. Rev. B **70**, 214422 (2004).
[27] O.Perković, K.A.Dahmen, and J.P.Sethna, cond-mat/9609072 (1996).
[28] For a discussion of the problems in the non-diluted 2d RFIM, see Ref. 27.